

Real-Space Berry Phases – Skyrmion Soccer

Karin Everschor-Sitte¹ and Matthias Sitte¹

The University of Texas at Austin, Department of Physics, 2515 Speedway, Austin, TX 78712, USA

(Dated: 6 May 2014)

Berry phases occur when a system adiabatically evolves along a closed curve in parameter space. This tutorial-like article focuses on Berry phases accumulated in real space. In particular, we consider the situation where an electron traverses a smooth magnetic structure, while its magnetic moment adjusts to the local magnetization direction. Mapping the adiabatic physics to an effective problem in terms of emergent fields reveals that certain magnetic textures – skyrmions – are tailor-made to study these Berry phase effects.

Over the last decades physicists have realized that a seemingly harmless phase – the Berry phase – leads to a lot of interesting physical consequences like quantum,¹ anomalous,² topological,^{3,4} and spin⁵ Hall effects, electric polarization,⁶ orbital magnetism,⁷ quantum charge pumping,⁸ etc. (For a review of Berry phase effects on electronic properties see Ref. 9.) Combining the Berry phase concepts with the physics of an electric current traversing a peculiar whirl-like magnetic texture first discovered¹⁰ in 2009 – magnetic skyrmions – reveals the elegance of these phases in a vivid way.

This paper is structured as follows: First, we review the general concept of Berry phases and introduce the main formulas. In Sec. II, we focus on real-space Berry phase effects. Here we discuss the example of a free electron traversing a spatially or temporally inhomogeneous, smooth magnetic structure. In the adiabatic limit, the magnetic moment of the electron adjusts constantly to the local magnetization direction and thereby the electron picks up a Berry phase. To interpret the physical consequences of these Berry phases, we review the mapping onto a problem, where the electron moves in a uniform Zeeman magnetic field, but instead “feels” an emergent electric field and an emergent orbital magnetic field, leading, for example, to the topological Hall effect⁴. In Sec. III, we first introduce skyrmions in a formal way and then later focussing on skyrmions in magnetic systems, in particular those in a certain material class denoted as B20 materials. We discuss that those magnetic textures are tailor-made to observe the emergent electric fields introduced in Sec. II A. In Sec. III C we switch the perspective and discuss the back reaction of the electronic Berry phase effects on the skyrmion lattice.

I. BERRY PHASES

Berry phases occur in all parts of physics and arise whenever a system adiabatically evolves along a cyclic process \mathcal{C} in some parameter space \mathbf{X} . A simple classical example is the parallel transport of a vector along a closed curve on a sphere (see Fig. 1). Although the system returns to its initial state it acquires a geometric phase characterized by the enclosed area on the sphere (Gauss-Bonnet theorem).

A quantum-mechanical example is a system whose states are non-degenerate and which evolves adiabatically in the parameter space $\mathbf{X} = \mathbf{X}(t)$. In that case, the solution of the time-dependent Schrödinger equation $i\hbar\partial_t|\psi(t)\rangle = H(\mathbf{X}(t))|\psi(t)\rangle$ is given by¹¹

$$|\psi(t)\rangle = \sum_n a_n(t_0) e^{i\gamma_n(\mathcal{C})} e^{-\frac{i}{\hbar} \int_0^t dt' \epsilon_n(\mathbf{X}(t'))} |\psi_n(t)\rangle, \quad (1)$$

where $|\psi_n(t)\rangle$ and $\epsilon_n(\mathbf{X}(t))$ are the time-evolved eigenstates and energies of the Hamiltonian $H(\mathbf{X}(t))$, $|\psi(t_0)\rangle = \sum_n a_n(t_0) |\psi_n(t_0)\rangle$ defines the initial state, and $\gamma_n(\mathcal{C})$ is the famous Berry phase.

Formally, the Berry phase $\gamma_n(\mathcal{C})$ is given by the line integral of the so-called Berry connection $\mathcal{A}_n(\mathbf{X})$ along the closed path \mathcal{C} :

$$\gamma_n(\mathcal{C}) = \oint_{\mathcal{C}} \mathcal{A}_n(\mathbf{X}) \cdot d\mathbf{X}, \quad (2)$$

$$\mathcal{A}_n(\mathbf{X}) = i \langle \psi_n | \nabla_{\mathbf{X}} | \psi_n \rangle. \quad (3)$$

Since the latter is a gauge-dependent vector-valued quantity it is also referred to as the Berry vector potential, in analogy to electrodynamics. The Berry phase, however, as a closed contour integral is independent of the gauge choice up to integer multiples of 2π . By means of Stokes theorem one can reformulate the Berry phase in terms of a surface integral. For a three dimensional parameter space \mathbf{X} this defines the so-called Berry curvature

$$\Omega_n(\mathbf{X}) = \nabla_{\mathbf{X}} \times \mathcal{A}_n(\mathbf{X}) \quad (4)$$

which takes a similar role as the magnetic field in electrodynamics (see below). The generalization of the Berry curvature to an arbitrary-dimensional parameter space is given by the antisymmetric rank-2 Berry curvature tensor $\Omega_{\mu\nu}(\mathbf{X}) = \partial_{X^\mu} \mathcal{A}_\nu - \partial_{X^\nu} \mathcal{A}_\mu$, where $\Omega_{\mu\nu} = \epsilon_{\mu\nu\xi} (\Omega_n)_\xi$.

So far we have not specified the parameter space \mathbf{X} . In general, position and momentum degrees of freedom are coupled and therefore real-space, momentum-space, and even mixed Berry phases occur simultaneously.^{9,12} In this paper, we focus on the limit, where mainly effects arising from Berry phases collected in real-space are important.

II. REAL-SPACE BERRY PHASES

An archetypical example of real-space Berry phase physics is a free electron traversing a spatially or tempo-

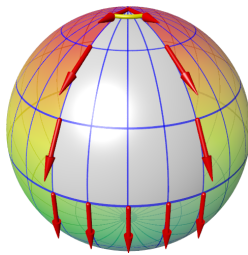


FIG. 1. (Color online) Parallel transport of a vector along a closed path on the sphere S_2 leads to a geometric phase between initial and final state.

rally inhomogeneous, smooth magnetic texture $\mathbf{M}(\mathbf{r}, t)$ with constant amplitude $M = |\mathbf{M}(\mathbf{r}, t)|$:

$$i\hbar\partial_t|\psi\rangle = \left[\frac{\mathbf{p}^2}{2m}\mathbb{1} - J\boldsymbol{\mu} \cdot \mathbf{M}(\mathbf{r}, t) \right] |\psi\rangle. \quad (5)$$

Here, $\psi = (\psi_\uparrow, \psi_\downarrow)^T$ is the two-component wave function, $\mathbb{1}$ is the 2×2 unit matrix, $J > 0$ is the strength of the ferromagnetic exchange coupling, and $\boldsymbol{\mu}$ is the magnetic moment of the electron. Note that for a particle with mass m , charge q , and Landé factor g the magnetic moment $\boldsymbol{\mu}$ and the spin \mathbf{s} are related by $\boldsymbol{\mu} = -(gq)/(2m)\mathbf{s}$. In particular, for a free electron with charge $q = -e$ the magnetic moment and the spin are antiparallel:

$$\boldsymbol{\mu} = -\frac{ge}{2m}\mathbf{s} = -\frac{g\mu_B}{2}\boldsymbol{\sigma}, \quad (6)$$

where μ_B is the Bohr magneton, and $\boldsymbol{\sigma} = (\sigma_x, \sigma_y, \sigma_z)^T$ denotes the vector of Pauli matrices. In a ferromagnetic material, the finite magnetization allows to define majority (minority) spins whose magnetic moments are parallel (antiparallel) to the magnetization direction. Historically, in the magnetic materials community the majority and minority spins are referred to as “spin-up” and “spin-down” states, while in the semiconductor community “spin-up” and “spin-down” refers to the actual orientation of the electron spin. Here, we follow the latter nomenclature.

In the adiabatic limit, the magnetic moment of the electron adapts constantly according to the local magnetization direction, and thereby the electron picks up a Berry phase.^{3,11,13–16} From this point of view, the physical consequences of the real-space Berry phase are “hidden” in the spatially and temporally varying spin states which enter the Berry vector potential [see Eq. (3)], $\mathcal{A}_\sigma = i\langle\psi_\sigma|\nabla|\psi_\sigma\rangle$ with $\sigma = \uparrow, \downarrow$ representing minority and majority spins, respectively. Note that minority and majority spins acquire opposite Berry phases when traversing a magnetic texture.

A. Alternative picture: emergent fields

An intuitive way to understand this adiabatic Berry phase physics is to consider a mapping onto a problem,

where the electron moves in a uniform Zeeman magnetic field, but instead “feels” an additional emergent electric field \mathbf{E}^e and an additional emergent (orbital) magnetic field \mathbf{B}^e .^{3,13,15–19}

$$\mathbf{B}_i^e = \frac{\hbar}{2}\epsilon_{ijk}\hat{\mathbf{M}} \cdot (\partial_j\hat{\mathbf{M}} \times \partial_k\hat{\mathbf{M}}), \quad (7a)$$

$$\mathbf{E}_i^e = \hbar\hat{\mathbf{M}} \cdot (\partial_i\hat{\mathbf{M}} \times \partial_t\hat{\mathbf{M}}), \quad (7b)$$

where $\partial_i = \partial/\partial r_i$, and $\hat{\mathbf{M}}(\mathbf{r}, t) = \mathbf{M}(\mathbf{r}, t)/M$ is the local magnetization direction. It is important to note that these emergent fields lead to Lorentz forces on the electrons that can be measured in experiments. For example, the emergent magnetic field leads directly to a contribution to the Hall signal. Since the profile of the magnetization configuration enters in \mathbf{B}^e , this type of Hall signal can be denoted as a geometrical Hall effect. In cases, where the magnetic texture is topologically nontrivial, it is commonly referred to the topological Hall effect. Note that the emergent electric field \mathbf{E}^e is only finite for a non-collinear, time-dependent magnetic texture. In Sec. III B, we discuss the situation of a moving magnetic texture and its consequences for the corresponding Hall signal.

In the following, we derive the above emergent fields following Ref. 18 and show that the emergent magnetic field is indeed the real-space Berry curvature.²⁰ The idea is to perform a *local* transformation $\psi = U(\mathbf{r}, t)\zeta$, so that the second part of the Hamiltonian becomes trivial:

$$-J\boldsymbol{\mu} \cdot \mathbf{M}(\mathbf{r}, t) = \tilde{J}\boldsymbol{\sigma} \cdot \hat{\mathbf{M}}(\mathbf{r}, t) \xrightarrow{U(\mathbf{r}, t)} \tilde{J}\sigma_z, \quad (8)$$

with $\tilde{J} = Jg\mu_B(\hbar/2)M > 0$. Hence, one has to rotate the quantization axis from the $\hat{\mathbf{z}}$ -direction to the local magnetization direction $\hat{\mathbf{M}}(\mathbf{r}, t)$. Such a unitary transformation U is given by

$$U = e^{-i(\theta/2)\boldsymbol{\sigma} \cdot \mathbf{n}} = \cos(\theta/2)\mathbb{1} - i\sin(\theta/2)\boldsymbol{\sigma} \cdot \mathbf{n}, \quad (9)$$

where $\theta = \arccos(\hat{\mathbf{M}} \cdot \hat{\mathbf{z}})$ is the angle of rotation, and $\mathbf{n} = \hat{\mathbf{z}} \times \hat{\mathbf{M}}/|\hat{\mathbf{z}} \times \hat{\mathbf{M}}|$ is the rotation axis. Note that we have dropped the explicit space and time dependence to simplify the notation. Multiplying Eq. (5) by U^\dagger from the left and inserting $\psi = U\zeta$ leads to a Schrödinger equation for ζ of the following form:

$$i\hbar\partial_t\zeta = \left[q^e V^e + \frac{(\mathbf{p}\mathbb{1} - q^e \mathbf{A}^e)^2}{2m} + \tilde{J}\sigma_z \right] \zeta. \quad (10)$$

By analogy to the Hamiltonian of a free electron under the influence of an electric and orbital magnetic field one can denote the 2×2 matrices

$$V^e = -(i\hbar/q^e)U^\dagger\partial_t U, \quad (11a)$$

$$\mathbf{A}^e = (i\hbar/q^e)U^\dagger\nabla U \quad (11b)$$

as the emergent “scalar” and “vector” potentials. At this level the emergent charge q^e is introduced artificially and actually drops out of Eq. (10). Furthermore, note that this transformation is exact.

For a magnetization texture $\mathbf{M}(\mathbf{r}, t)$ which varies smoothly in space and time, one can treat the scalar and vector potentials V^e and \mathbf{A}^e as a perturbation to the unperturbed Hamiltonian $H_0 = \mathbf{p}^2/(2m)\mathbb{1} + \tilde{J}\sigma_z$. In the adiabatic approximation, V^e and \mathbf{A}^e act on each band separately, allowing us to introduce electromagnetic potentials for both bands:

$$\mathcal{A}_\sigma^e = \langle \sigma | \mathbf{A}^e | \sigma \rangle = (i\hbar/q^e) \langle \psi_\sigma | \nabla | \psi_\sigma \rangle, \quad (12a)$$

$$\mathcal{V}_\sigma^e = \langle \sigma | V^e | \sigma \rangle = -(i\hbar/q^e) \langle \psi_\sigma | \partial_t | \psi_\sigma \rangle, \quad (12b)$$

with $\sigma = \uparrow, \downarrow$ for minority and majority spins, respectively, and $|\psi_\sigma\rangle = U|\sigma\rangle$. Above potentials have the same form of the Berry vector potential introduced in Eq. (3).

Finally, introducing for each band an emergent electric field, $\mathbf{E}_\sigma^e = -\nabla \mathcal{V}_\sigma^e - \partial_t \mathcal{A}_\sigma^e$, and an emergent magnetic field, $\mathbf{B}_\sigma^e = \nabla \times \mathcal{A}_\sigma^e$, that are “felt” by the electron, it becomes clear that the real-space Berry curvature acts like an emergent magnetic field, while the mixed space-time Berry curvature acts like an emergent electric field. By an explicit calculation one finds

$$(\mathbf{B}_\sigma^e)_i = \mp \frac{\hbar}{2q^e} \frac{\epsilon_{ijk}}{2} \hat{\mathbf{M}} \cdot (\partial_j \hat{\mathbf{M}} \times \partial_k \hat{\mathbf{M}}), \quad (13a)$$

$$(\mathbf{E}_\sigma^e)_i = \mp \frac{\hbar}{2q^e} \hat{\mathbf{M}} \cdot (\partial_i \hat{\mathbf{M}} \times \partial_t \hat{\mathbf{M}}), \quad (13b)$$

where the upper (lower) sign corresponds to the band for electrons with minority (majority) spin. Let us now assign different emergent charges to the two bands, because the sign of the Berry phase depends on the orientation of the spin.²¹ For a minority (majority) spin we define²² $q_\uparrow^e = -1/2$ ($q_\downarrow^e = 1/2$), leading to the emergent fields given in Eq. (7).

In principle, any magnetic structure that varies smoothly in position space leads to an emergent magnetic field [Eq. (7a)] and thus to a geometrical Hall effect. As it turns out, there are ideal magnetic textures – skyrmions – which are tailored to investigate these emergent fields.

III. SKYRMIONS

Like the concept of the Berry phase, a skyrmion is a certain mathematical object which is realized in many areas of physics ranging from nuclear and particle physics over high-energy physics to condensed matter physics. It is named after the nuclear physicist Tony Skyrme who in the early 1960’s studied a certain nonlinear field theory for interacting pions, showing that quantized and topologically stable field configurations – nowadays called skyrmions – do occur as solutions of such field theories.²³ In the original work, Skyrme considered three-dimensional versions of skyrmions, but later the notion of a skyrmion was generalized to arbitrary dimensions: One can define a skyrmion as a topologically stable, smooth field configuration describing a non-trivial surjective mapping from coordinate space to an order parameter space with a non-trivial topology. In the following, we restrict the discussion to the two-dimensional

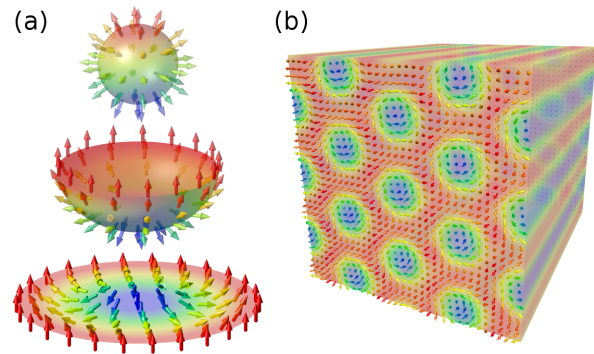


FIG. 2. (Color online) (a) A (non-chiral) skyrmion configuration (bottom) is obtained by “unfolding” a hedgehog (top). Arrows correspond to the local magnetization direction $\hat{\mathbf{M}} = \mathbf{M}/|\mathbf{M}|$. The color code is chosen according to the out-of-plane component of the arrows: from red (“up”) over green (in-plane) to blue (“down”). (b) Schematic plot of a chiral skyrmion lattice with an additional in-plane winding of the magnetization.

unit sphere, S_2 , describing the magnetization direction $\hat{\mathbf{M}}$. An intuitive picture of a skyrmion and the mapping to a sphere is shown in Fig. 2 (a), where “infinity” (the boundary of the skyrmion) is mapped onto the north pole. Note that a skyrmion is everywhere non-singular and finite. In contrast to vortices, skyrmions are trivial at infinity, *i.e.*, all arrows at the boundary point in the same direction out of plane.

At the end of the 1980’s skyrmion structures were shown to be the mean-field ground states of certain models for anisotropic, non-centrosymmetric magnetic materials with chiral spin-orbit interactions subjected to a magnetic field.²⁴ Although some further theoretical works appeared on magnetic skyrmions and similar textures,^{16,25} the real breakthrough was in 2009 when a hexagonal lattice of skyrmion-tubes perpendicular to a finite, external magnetic field [as sketched in Fig. 2 (b)] was experimentally discovered in the cubic helimagnet manganese silicide (MnSi).¹⁰ Since 2009 skyrmions have been observed in many other B20 compounds^{4,26,27}, including metals, semiconductors, and also an insulating, multiferroic material.²⁸ The skyrmion lattice was also confirmed to exist in thin films by a direct imaging of the real-space magnetic texture by Lorentz transmission electron microscopy.^{29,30} Moreover, skyrmion textures have been discussed in thin films in the form of magnetic bubble domains.³¹ Furthermore, skyrmions have been found on surfaces as a spontaneous magnetic ground state forming a lattice on the atomic scale.³²

In skyrmion lattices, different length scales appear:^{10,33} the size of the atomic unit cell corresponding to the wavelength of the electrons, the diameter of the skyrmions, the (non-spinflip) mean-free path, and the much larger spinflip scattering length. In the adiabatic limit, where the size of the skyrmions is much larger than the non-spinflip scattering length, band structure effects are negligible,

and one can concentrate on real-space Berry phases.³³ In the opposite limit, band structure effects are expected to dominate, and momentum-space Berry phases become relevant.³³

In B20 structures like MnSi a hierarchy of energy scales exists which also determines the size of the skyrmion structures: ferromagnetic exchange coupling, Dzyaloshinskii-Moriya interaction, and crystalline field interactions. Since the ratio of the Dzyaloshinskii-Moriya and the ferromagnetic exchange interaction is small in B20 structures, the diameter of a skyrmion is much larger than the crystallographic unit cell, and the skyrmion textures are smooth. Consequently, those magnetic structures are good candidates to study the physics of real-space Berry phases.

A. Winding number and emergent magnetic field

Skyrmions can be classified according to their integer winding number \mathcal{W} counting the number of times the field configuration wraps around the whole sphere. To obtain the winding number of a magnetization configuration which varies in the xy plane as the example shown in the bottom panel of Fig. 2 (a), one has to integrate the solid angle swept out by $\hat{\mathbf{M}}$:

$$\mathcal{W} = \frac{1}{4\pi} \int \hat{\mathbf{M}} \cdot (\partial_x \hat{\mathbf{M}} \times \partial_y \hat{\mathbf{M}}) dx dy. \quad (14)$$

Comparing the winding number with the emergent fields [cf. Eq. (7)] one observes that the emergent magnetic field is of particular interest for the skyrmion lattice: The topology of the skyrmion ensures the “emergent magnetic flux” per unit cell to be quantized, as can be seen by integrating Eq. (7a) over a magnetic unit cell (UC):

$$\int_{\text{UC}} \mathbf{B}^e \cdot d\boldsymbol{\sigma} = 4\pi\hbar\mathcal{W}, \quad (15)$$

with $\mathcal{W} = -1$ for skyrmions in the chiral magnet MnSi^{4,10,29} where the z axis is along the external magnetic field direction. The topological Hall effect due to the emergent magnetic field was one of the first experimental confirmations that the magnetic textures observed in MnSi and other B20 structures have a topological character and are actually lattices of skyrmion tubes.^{4,34} Note that the emergent fields (7) have been derived for a simple model, and therefore only a qualitative understanding of the experimental signatures is possible at this level. To obtain a quantitative agreement with experiments corrections due to non-adiabatic processes^{21,35}, fluctuations of the magnetization amplitude, modifications due to the band structure, etc. have to be taken into account.

B. Moving skyrmions and emergent electric field

As mentioned above, to observe the emergent electric field a time-dependent magnetic texture is needed. One way to obtain a moving magnetic texture is to exploit the spin-torque effect³⁶ by sending a sufficiently large spin-polarized current through the sample which “pushes” the magnetic structure forward. Usually a spin polarized current is obtained by sending an electric current through a sample with a finite magnetic moment, but there are also other options to create spin currents like thermal or magnetic field gradients or via the intrinsic spin Hall effect.^{5,37} The spin torque effect allows, for example, to move ferromagnetic domain walls³⁸ with the potentially application of racetrack memories.³⁹ However, the threshold current density, above which the domain walls get unpinned from disorder, is very high, $j_c \sim 10^{11}$ A/m².

A key feature of the smooth skyrmion lattice in chiral magnets is the very efficient coupling to electric currents. This is reflected in an ultra-low threshold current density above which the skyrmion lattice starts moving. For example, in MnSi,^{21,40} the threshold current density is five orders of magnitude smaller compared to the one for traditional spin-torque effects, $j_c \sim 10^6$ A/m².

For current densities well above the threshold current density, a rigid skyrmion lattice moves mainly along the current direction with a drift velocity \mathbf{v}_d , and the relative speed between the spin current and the magnetic structure is reduced.^{21,41–43} For a rigid drifting magnetic texture with $\hat{\mathbf{M}}(\mathbf{r}, t) = \hat{\mathbf{M}}(\mathbf{r} - \mathbf{v}_d t)$ the emergent electric and magnetic fields [Eq. (7)] are coupled since $\partial_t \hat{\mathbf{M}} = -(\mathbf{v}_d \cdot \nabla) \hat{\mathbf{M}}$:

$$\mathbf{E}^e = -\mathbf{v}_d \times \mathbf{B}^e. \quad (16)$$

Thus, one can identify the emergent electric field of the skyrmion lattice by a reduction of the Hall signal,^{19,21} because the effective forces on the electrons due to the emergent electric field are basically in opposite direction than the ones due to the emergent magnetic field. Note that Eq. (16) reflects Faraday’s law of induction, indicating that a change of the magnetic flux causes an electric field. Another interesting aspect is that one can determine the drift velocity \mathbf{v}_d from the same Hall measurement by virtue of Eq. (16) since the emergent magnetic field of the skyrmion lattice is quantized. For more details and experimental results see, *e.g.*, Ref. 21.

C. Spintronics with skyrmions

So far we have discussed the Berry phase physics a conduction electron experiences when traversing a spatially and temporally inhomogeneous, smooth magnetic texture. Let us now switch the perspective and consider the effects of the electrons on the magnetic texture. The magnetization dynamics can be modeled within the Landau-Lifshitz-Gilbert equation, an effective equation

of motion for the slowly and smoothly varying magnetization direction of a magnetic texture with constant amplitude.^{36,44} Here, we will not discuss the magnetization dynamics in detail, but rather consider the current-induced forces on a skyrmion texture from a qualitative point of view. The equation of the forces (per skyrmion, per length, and per \hbar) acting on the skyrmion lattice can be obtained from the Landau-Lifshitz-Gilbert equation using the Thiele method and treating pinning physics phenomenologically (see, *e.g.*, Refs. 21,41,42):

$$\mathcal{D}(\tilde{\beta}\mathbf{v}_s - \tilde{\alpha}\mathbf{v}_d) + \mathbf{G} \times (\mathbf{v}_s - \mathbf{v}_d) + \mathbf{F}_{\text{pin}} = 0. \quad (17)$$

Here, \mathcal{D} is the dissipative tensor, $\tilde{\alpha}$ and $\tilde{\beta}$ are effective damping parameters, \mathbf{v}_s is an effective spin velocity, \mathbf{v}_d is the drift velocity of the magnetic texture, \mathbf{G} is the gyrocoupling vector, and \mathbf{F}_{pin} is the phenomenological pinning force.

Basically there are three different types of forces acting on the skyrmion lattice when subjected to an electric current: two types of current-induced forces (schematically shown in the right panel of Fig. 3, for a non-moving skyrmion) and pinning forces. In the absence of a current ($\mathbf{v}_s = 0$), the skyrmion lattice is pinned by impurities and the underlying atomic lattice, *i.e.*, $\mathbf{v}_d = 0$. Turning on the electric current, the current-induced forces are first fully compensated by the pinning force \mathbf{F}_{pin} .⁴⁵ For larger current densities, the current-induced forces overcome the pinning forces and induce a translational motion of the magnetic texture: The first term of Eq. (17) describes a dissipative or drag force dragging the skyrmion lattice along the direction of the spin-current, while the second term of Eq. (17) describes a force on the magnetic texture, which is commonly referred to as a Magnus force. It can be understood (according to Newton's third law) as the counter-force on the magnetic texture opposite to the Lorentz force on the electrons due to the emergent electric fields. Hence, this Magnus force is related to Berry phase physics, and occurs, in principle, for any inhomogeneous magnetic texture. However, it is not surprising that the Magnus force is also particularly interesting in skyrmion lattices due to their topology. For the case of the skyrmion lattice, the gyrocoupling can be explicitly expressed in terms of the emergent magnetic field, $\mathbf{G} = \int_{UC} d^2r M \mathbf{B}^e \sim \mathcal{W}$, and is thus proportional to the winding number:^{40,46} Thus, for zero drift velocity the Magnus force is perpendicular to the direction of the spin current.

Note that the notion of a Magnus force is chosen in analogy to classical mechanics where, for example, the Magnus force acting on a spinning ball in viscous air leads to a bending of the ball's flight path (see Fig. 3, left panel) – famous examples are “banana kicks” in soccer. In the rest-frame of the ball, the origin of the Magnus force (depicted as the red thick arrow in the left panel of Fig. 3) can be understood on a fairly simple level: For a non-spinning ball, the air passes the ball on both sides equally fast, and thus there are no net forces acting on the ball in perpendicular direction. However, for a rotating

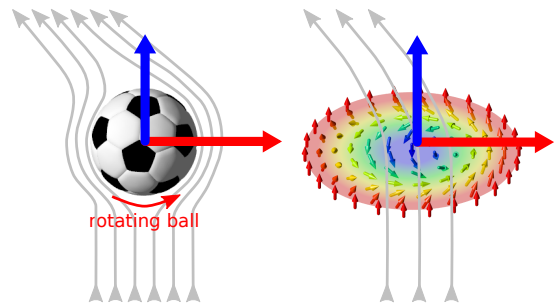


FIG. 3. Sketch of the current-induced forces acting on a skyrmion (right panel) in comparison with the forces acting on a spinning ball in viscous air (left panel).

ball the air is accelerated on one side and decelerated on the other side so that the air is deflected. As the air experiences a force, the ball experiences the opposite force – the Magnus force – according to Newton's third law.

In the skyrmion case it is the Lorentz force induced by the emergent magnetic field that deflects the current and which in turn leads to a counter-effect – the Magnus force – on the magnetic texture. Note, however, that this analogy is not complete, because, *e.g.*, spin is not a conserved quantity. Nevertheless, this picture helps to understand why skyrmion lattices couple efficiently to electric currents. Current-induced spin-torque effects occur only when the magnetization changes in space or time. For spin structures like magnetic domain walls this is only a nanoscopic region, while in the skyrmion lattice the smooth twist of the local magnetization extends over macroscopic magnetic domains. In addition, a weak coupling to the underlying atomic lattice¹⁰ and a small pinning to disorder⁴³ leads to the very low threshold current density for the smooth skyrmion lattice.^{21,40} This excellent coupling to electric currents makes skyrmion systems very interesting to study spin-torque effects as effects like Joule heating and Oersted magnetic fields created by the current are less disturbing. Furthermore, it allows for fundamental spin-torque experiments in bulk materials, where surface effects that dominate in nanoscopic samples are small.

With that knowledge about skyrmions, their excitations⁴⁷, and how to move,²¹ rotate,^{40,42} and even merge them,⁴⁸ skyrmions are not only a powerful laboratory system to study fundamental physics, but may really become relevant for technological applications. Keeping skyrmion spintronics in mind, small devices and thus small magnetic textures (where also momentum space Berry phases are potentially relevant) are of course desired. Experimentally, it has been shown that the size of the skyrmions can be controlled to some extent by doping within the B20 structures.²⁶ On the atomic scale, skyrmions have been observed as the ground state of an Fe film on Ir(111) substrates.³² As a starting point for magnetic storage technologies, the same group has recently achieved to write and erase

single skyrmions by surface techniques.⁴⁹ Furthermore, a potential generalization of racetrack memories using skyrmions has been recently proposed and investigated within micromagnetic simulations.⁵⁰ As those magnetic skyrmions are of two-dimensional nature, it might also be interesting to look for new, two-dimensional storage devices, where the intrinsic properties of the skyrmions can be used even better.

To summarize, skyrmions exhibit a lot of exciting physics and are tailored to study Berry-phase and spin-torque effects.

ACKNOWLEDGMENTS

We thank Achim Rosch and Christian Pfleiderer for continuous great support. This work was supported by a fellowship within the postdoc program of the German Academic Exchange Service (DAAD). Financial support from the Deutsche Telekom-Stiftung (KE) is gratefully acknowledged.

- ¹D. J. Thouless, M. Kohmoto, M. P. Nightingale, and M. den Nijs, *Phys. Rev. Lett.* **49**, 405 (1982).
- ²N. Nagaosa, J. Sinova, S. Onoda, A. H. MacDonald, and N. P. Ong, *Rev. Mod. Phys.* **82**, 1539 (2010).
- ³P. Bruno, V. K. Dugaev, and M. Taillefumier, *Phys. Rev. Lett.* **93**, 096806 (2004); M. Onoda, G. Tatara, and N. Nagaosa, *J. Phys. Soc. Jpn.* **73**, 2624 (2004).
- ⁴A. Neubauer, C. Pfleiderer, B. Binz, A. Rosch, R. Ritz, P. G. Niklowitz, and P. Böni, *Phys. Rev. Lett.* **102**, 186602 (2009).
- ⁵S. Murakami, N. Nagaosa, and S.-C. Zhang, *Science* **301**, 1348 (2003); J. Sinova, D. Culcer, Q. Niu, N. A. Sinitsyn, T. Jungwirth, and A. H. MacDonald, *Phys. Rev. Lett.* **92**, 126603 (2004); D. Culcer, J. Sinova, N. A. Sinitsyn, T. Jungwirth, A. H. MacDonald, and Q. Niu, *Phys. Rev. Lett.* **93**, 046602 (2004).
- ⁶R. D. King-Smith and D. Vanderbilt, *Phys. Rev. B* **47**, 1651 (1993); R. Resta, *Rev. Mod. Phys.* **66**, 899 (1994).
- ⁷T. Thonhauser, D. Ceresoli, D. Vanderbilt, and R. Resta, *Phys. Rev. Lett.* **95**, 137205 (2005); D. Xiao, J. Shi, and Q. Niu, *Phys. Rev. Lett.* **95**, 137204 (2005).
- ⁸D. J. Thouless, *Phys. Rev. B* **27**, 6083 (1983).
- ⁹D. Xiao, M.-C. Chang, and Q. Niu, *Rev. Mod. Phys.* **82**, 1959 (2010).
- ¹⁰S. Mühlbauer, B. Binz, F. Jonietz, C. Pfleiderer, A. Rosch, A. Neubauer, R. Georgii, and P. Böni, *Science* **323**, 915 (2009).
- ¹¹M. V. Berry, *Proc. R. Soc. Lond. A* **392**, 45 (1984).
- ¹²F. Freimuth, R. Bamler, Y. Mokrousov, and A. Rosch, [arXiv:1307.8085](https://arxiv.org/abs/1307.8085) (2013).
- ¹³J. Ye, Y. B. Kim, A. J. Millis, B. I. Shraiman, P. Majumdar, and Z. Tešanović, *Phys. Rev. Lett.* **83**, 3737 (1999).
- ¹⁴Y. Taguchi, Y. Oohara, H. Yoshizawa, N. Nagaosa, and Y. Tokura, *Science* **30**, 2573 (2001).
- ¹⁵G. Tatara, H. Kohno, J. Shibata, Y. Lemaho, and K.-J. Lee, *J. Phys. Soc. Jpn.* **76**, 054707 (2007).
- ¹⁶B. Binz and A. Vishwanath, *Phys. B* **403**, 1336 (2008).
- ¹⁷G. E. Volovik, *J. Phys. C: Solid State Physics* **20**, L83 (1987); S. E. Barnes and S. Maekawa, *Phys. Rev. Lett.* **98**, 246601 (2007); S. A. Yang, G. S. D. Beach, C. Knutson, D. Xiao, Q. Niu, M. Tsoi, and J. L. Erskine, *Phys. Rev. Lett.* **102**, 067201 (2009).
- ¹⁸S. Zhang and S. S.-L. Zhang, *Phys. Rev. Lett.* **102**, 086601 (2009).
- ¹⁹J. Zang, M. Mostovoy, J. H. Han, and N. Nagaosa, *Phys. Rev. Lett.* **107**, 136804 (2011).
- ²⁰Ref. 18 employs a different sign convention and does not use the Einstein sum convention.
- ²¹T. Schulz, R. Ritz, A. Bauer, M. Halder, M. Wagner, C. Franz, C. Pfleiderer, K. Everschor, M. Garst, and A. Rosch, *Nat. Phys.* **8**, 301 (2012).
- ²²Signs for q_{σ}^e are opposite as in Ref. 21.
- ²³T. H. R. Skyrme, *Proc. R. Soc. A* **260**, 127 (1961); *Nucl. Phys.* **31**, 556 (1962).
- ²⁴A. N. Bogdanov and D. A. Yablonskii, *Sov. Phys. JETP* **68**, 101 (1989); A. N. Bogdanov and A. Hubert, *J. Magn. Magn. Mater.* **138**, 255 (1994); A. N. Bogdanov, *Sov. Phys. JETP* **62**, 247 (1995).
- ²⁵B. Binz, A. Vishwanath, and V. Aji, *Phys. Rev. Lett.* **96**, 207202 (2006); B. Binz and A. Vishwanath, *Phys. Rev. B* **74**, 214408 (2006); U. K. Rößler, A. N. Bogdanov, and C. Pfleiderer, *Nature* **442**, 797 (2006); I. Fischer, N. Shah, and A. Rosch, *Phys. Rev. B* **77**, 024415 (2008); S. D. Yi, S. Onoda, N. Nagaosa, and J. H. Han, *Phys. Rev. B* **80**, 054416 (2009); J. H. Han, J. Zang, Z. Yang, J.-H. Park, and N. Nagaosa, *Phys. Rev. B* **82**, 094429 (2010).
- ²⁶W. Münzer, A. Neubauer, T. Adams, S. Mühlbauer, C. Franz, F. Jonietz, R. Georgii, P. Böni, B. Pedersen, M. Schmidt, A. Rosch, and C. Pfleiderer, *Phys. Rev. B* **81**, 041203 (2010); K. Shibata, X. Z. Yu, T. Hara, D. Morikawa, N. Kanazawa, K. Kimoto, S. Ishiwata, Y. Matsui, and Y. Tokura, *Nat. Nano advance online publication* (2013), 10.1038/nnano.2013.174.
- ²⁷C. Pfleiderer, T. Adams, A. Bauer, W. Biberacher, B. Binz, F. Birkelbach, P. Böni, C. Franz, R. Georgii, M. Janoschek, F. Jonietz, T. Keller, R. Ritz, S. Mühlbauer, W. Münzer, A. Neubauer, B. Pedersen, and A. Rosch, *J. Phys.: Condens. Matter* **22**, 164207 (2010).
- ²⁸S. Seki, X. Z. Yu, S. Ishiwata, and Y. Tokura, *Science* **336**, 198 (2012); T. Adams, A. Chacon, M. Wagner, A. Bauer, G. Brandl, B. Pedersen, H. Berger, P. Lemmens, and C. Pfleiderer, *Phys. Rev. Lett.* **108**, 237204 (2012).
- ²⁹X. Z. Yu, Y. Onose, N. Kanazawa, J. H. Park, J. H. Han, Y. Matsui, N. Nagaosa, and Y. Tokura, *Nature* **465**, 901 (2010).
- ³⁰X. Z. Yu, Y. Onose, N. Kanazawa, J. H. Park, J. H. Han, Y. Matsui, N. Nagaosa, and Y. Tokura, *Nat. Mat.* **10**, 106 (2011); X. Z. Yu, N. Kanazawa, W. Z. Zhang, T. Nagai, T. Hara, K. Kimoto, Y. Matsui, Y. Onose, and Y. Tokura, *Nat. Commun.* **3**, 988 (2012).
- ³¹A. Malozemoff and J. Slonczewski, *Magnetic domain walls in bubble materials* (Academic Press, 1979); X. Yu, M. Mostovoy, Y. Tokunaga, W. Zhang, K. Kimoto, Y. Matsui, Y. Kaneko, N. Nagaosa, and Y. Tokura, *Proc. Natl. Acad. Sci. USA* **109**, 8856 (2012).
- ³²S. Heinze, K. von Bergmann, M. Menzel, J. Brede, A. Kubetzka, R. Wiesendanger, G. Bihlmayer, and S. Blügel, *Nat. Phys.* **7**, 713 (2011).
- ³³N. Nagaosa, X. Z. Yu, and Y. Tokura, *Phil. Trans. R. Soc. A* **370**, 5806 (2012).
- ³⁴M. Lee, W. Kang, Y. Onose, Y. Tokura, and N. P. Ong, *Phys. Rev. Lett.* **102**, 186601 (2009).
- ³⁵J. Xiao, A. Zangwill, and M. D. Stiles, *Phys. Rev. B* **73**, 054428 (2006).
- ³⁶J. C. Slonczewski, *J. Magn. Magn. Mat.* **159**, L1 (1996); L. Berger, *Phys. Rev. B* **54**, 9353 (1996).
- ³⁷M. I. Dyakonov and V. I. Perel, *Phys. Lett. A* **35**, 459 (1971); J. E. Hirsch, *Phys. Rev. Lett.* **83**, 1834 (1999); S. Zhang, *Phys. Rev. Lett.* **85**, 393 (2000); J. Sinova, S. Murakami, S.-Q. Shen, and M.-S. Choi, *Sol. St. Comm.* **138**, 214 (2006).
- ³⁸J. Grollier, P. Boulenc, V. Cros, A. Hamzi, A. Vaurs, A. Fert, and G. Faini, *Appl. Phys. Lett.* **83**, 509 (2003); M. Tsoi, R. E. Fontana, and S. S. P. Parkin, *Science* **83**, 2617 (2003).
- ³⁹S. S. P. Parkin, M. Hayashi, and L. Thomas, *Science* **320**, 190 (2008).
- ⁴⁰F. Jonietz, S. Mühlbauer, C. Pfleiderer, A. Neubauer, W. Münzer, A. Bauer, T. Adams, R. Georgii, P. Böni, R. A. Duine, K. Everschor, M. Garst, and A. Rosch, *Science* **330**, 1648 (2010).

- ⁴¹K. Everschor, Ph.D. thesis, Institute of Theoretical Physics, University of Cologne (2012).
- ⁴²K. Everschor, M. Garst, B. Binz, F. Jonietz, S. Mühlbauer, C. Pfleiderer, and A. Rosch, *Phys. Rev. B* **86**, 054432 (2012).
- ⁴³J. Iwasaki, M. Mochizuki, and N. Nagaosa, *Nat. Commun.* **4**, 1463 (2013).
- ⁴⁴S. Zhang and Z. Li, *Phys. Rev. Lett.* **93**, 127204 (2004); R. A. Duine, A. S. Núñez, J. Sinova, and A. H. MacDonald, *Phys. Rev. B* **75**, 214420 (2007); M. E. Lucassen, H. J. van Driel, C. M. Smith, and R. A. Duine, *Phys. Rev. B* **79**, 224411 (2009).
- ⁴⁵In principle, there might be a tiny motion due to thermal (or quantum) fluctuations,⁵¹ so called creep, also below the critical current density, which is neglected here.
- ⁴⁶K. Everschor, M. Garst, R. A. Duine, and A. Rosch, *Phys. Rev. B* **84**, 064401 (2011).
- ⁴⁷O. Petrova and O. Tchernyshyov, *Phys. Rev. B* **84**, 214433 (2011); M. Mochizuki, *Phys. Rev. Lett.* **108**, 017601 (2012); Y. Onose, Y. Okamura, S. Seki, S. Ishiwata, and Y. Tokura, *Phys. Rev. Lett.* **109**, 037603 (2012); M. Mochizuki and S. Seki, *Phys. Rev. B* **87**, 134403 (2013).
- ⁴⁸P. Milde, D. Köhler, J. Seidel, L. M. Eng, A. Bauer, A. Chacon, J. Kindervater, S. Mühlbauer, C. Pfleiderer, S. Buhrandt, C. Schütte, and A. Rosch, *Science* **340**, 1076 (2013).
- ⁴⁹N. Romming, C. Hanneken, M. Menzel, J. E. Bickel, B. Wolter, K. von Bergmann, A. Kubetzka, and R. Wiesendanger, *Science* **341**, 636 (2013).
- ⁵⁰A. Fert, V. Cros, and J. Sampaio, *Nat. Nano* **8**, 152 (2013).
- ⁵¹G. Blatter, M. V. Feigel'man, V. B. Geshkenbein, A. I. Larkin, and V. M. Vinokur, *Rev. Mod. Phys.* **66**, 1125 (1994).